npj Computational Materials

www.nature.com/npjcompumats

ARTICLE OPEN

Check for updates

Nanometer-size Na cluster formation in micropore of hard carbon as origin of higher-capacity Na-ion battery

Yong Youn[1], Bo Gao[1], Azusa Kamiyama[2], Kei Kubota[2,3], Shinichi Komaba[2,3] and Yoshitaka Tateyama[1,3]✉

Development of high-energy-density anode is crucial for practical application of Na-ion battery as a post Li-ion battery. Hard carbon (HC), though a promising anode candidate, still has bottlenecks of insufficient capacity and unclear microscopic picture. Usage of the micropore has been recently discussed, however, the underlying sodiation mechanism is still controversial. Herein we examined the origin for the high-capacity sodiation of HC, based on density functional theory calculations. We demonstrated that nanometer-size Na cluster with 3–6 layers is energetically stable between two sheets of graphene, a model micropore, in addition to the adsorption and intercalation mechanisms. The finding well explains the extended capacity over typical 300 mAhg^{-1}, up to 478 mAhg^{-1} recently found in the MgO-templated HC. We also clarified that the MgO-template can produce suitable nanometer-size micropores with slightly defective graphitic domains in HC. The present study considerably promotes the atomistic theory of sodiation mechanism and complicated HC science.

npj Computational Materials (2021)7:48 ; https://doi.org/10.1038/s41524-021-00515-7

INTRODUCTION

Li-ion batteries (LIBs) have been widely used due to the lightweight, high-energy density, and rechargeability, and even Nobel prize in chemistry 2019 was awarded to the researchers for LIB[1–3]. In spite of the outstanding advantages of LIBs, their high price and limited quantities make it difficult to cope with the explosively increased usage for energy storage[4]. Recently, Na-ion batteries (NIBs) have been attracted as an alternative of LIBs[5,6]. Sodium is much cheaper and richer than Lithium. In addition, they have similar chemical properties since they belong to the same group, alkali metal. Thus, the exploration of cathode, anode, and electrolyte materials, referring to the knowledge for the LIBs, has been carried out. Then, several new transition metal oxides for the cathode (e.g., $Na_{2/3}Ni_{1/3}Mn_{1/2}Ti_{1/6}O_2$) and alloys for the anode have been proposed[7,8], in which the novel principles are involved due to the different ionic radius and ionization potential of Sodium.

The most representative difference is the carbon anode material. Graphite, which is widely used for the LIB anode[9], does not work well in NIBs[10], mainly because of no-intercalation preference of sodium into the graphite. Therefore, many researchers have attempted to discover alternative anodes for NIBs and the hard carbon (HC) turns out to be a candidate[10–12]. HC composed of disordered graphene sheets (or graphitic domains) exhibits outstanding properties such as reasonable capacity, sufficient potential, and cycling stability[11,13–15]. Along with improvement of the performance of HC, many studies have been conducted to reveal the fundamental mechanism of sodiation[16–24]. In 2000, Stevens et al. suggested "house of cards" model that is generally accepted today[16]. In the model, HC particles are composed of graphitic domains with a few layers of curved graphene and micropores surrounded by the graphitic domains as shown in Fig. 1a. Therefore, Na ions can be stored through the intercalation into the graphitic domains and the insertion in the micropores including the adsorption on the pore wall and clustering in the pore (see in Fig. 1b). Also, the ions can be adsorbed on the specific active sites such as defects, edges, and functional groups. The outer surface of HC particles is another region where the solid electrolyte interphase (SEI) is formed or sodium metal is plated, which is related to irreversible capacity or detrimental reactivity[25].

Even though most of the current studies are based on the "House of cards" model, there are several controversies about the details. One of the debates is about the origin of the slope (above 0.1 V) and plateau capacity (below 0.1 V) observed in a typical charge–discharge curve as shown in Fig. 1c. In some studies[16,17,22,26], they claimed that insertion of Na ions in the micropores is a dominant mechanism of the plateau capacity. Whereas, in the other literatures[20,21,24], intercalation into the graphitic domains is considered a main contributor to the plateau region. From electronic viewpoints, the emergence of the quasi-metallic Na states in the plateau region has been debated[21,27,28]. In addition, the difference of the quasi-metallic states from the Na plating on the HC particle surface is still an open question. Theoretical studies could be the key to solving the problem. For example, Tsai et al.[29] demonstrated that Na ions can be intercalated into the layered domain with defect or large interlayer space even though Na intercalation into the graphite is energetically unstable[30–33]. Also, the possibility of cluster adsorption on the surface has been reported[19,34,35]. Nonetheless, there are many unsolved questions such as the assignment of the mechanisms to the potential, the capacity limit of each sodiation mechanism, and the occurrence of Na cluster in the micropore. Furthermore, it is necessary to identify the origin of the extremely high capacity of recent MgO-templated HC[36] over typical 300 mAhg^{-1}, up to 478 mAhg^{-1} to design a novel high-capacity HC.

In this study, we investigate the microscopic origin of Na capacity in the HC and reveal the sodiation mechanism using density functional theory (DFT) calculations. Based on the "house

[1]Center for Green Research on Energy and Environmental Materials (GREEN) and International Center for Materials Nanoarchitectonics (MANA), National Institute for Materials Science (NIMS), Ibaraki, Japan. [2]Department of Applied Chemistry, Tokyo University of Science, Tokyo, Japan. [3]Elements Strategy Initiative for Catalysts and Batteries (ESICB), Kyoto University, Kyoto, Japan. ✉email: TATEYAMA.Yoshitaka@nims.go.jp

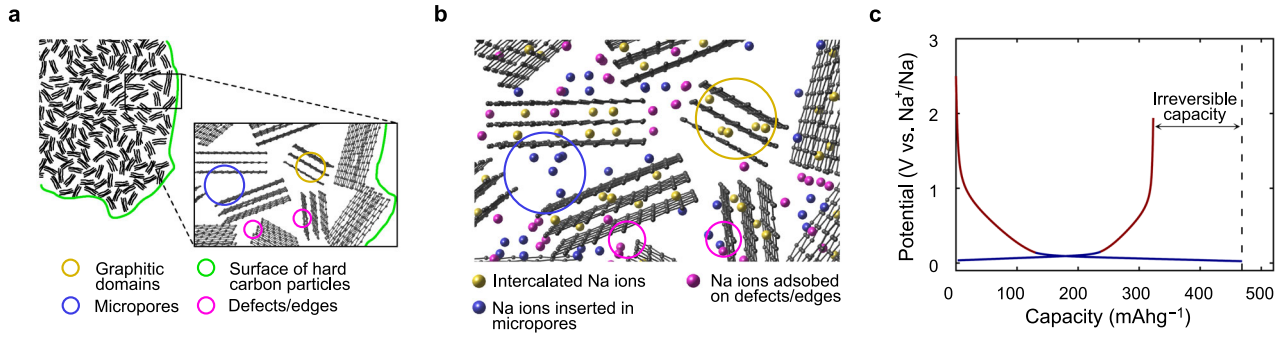

Fig. 1 Schematics related to the sodiation in HC. Schematic illustrations of **a** the structure of HC particle, **b** Na-ion storage in HC based on the house of cards model, and **c** typical charge–discharge curve with HC anode. The colors of Na ions in (**b**) are corresponding to the sodiation sites in (**a**).

of cards" model, we revisit the Na-storing mechanism in the slope and plateau regions in Fig. 1. In particular, we resolve the atomistic origin of the Na storage in the extended plateau region beyond 300 mAhg^{-1} observed in the experiments. Then we found that the nanometer-size Na cluster can be energetically stable in the micropore, which is in contrast to the unfavored Na intercalation into graphite, and that it has quasi-metallic character and the positive insertion potential w.r.t. Na/Na^{+} reference. Besides, we explore the MgO-template effect on the micropore formation of the HC via DFT molecular dynamics and demonstrate that the MgO microstructure can give many nanometer-scale micropores in fact. Based on these results, we discuss the sodiation mechanism and HC design principle for higher capacity theoretically.

RESULTS

Intercalation into the graphitic domains of hard carbon

We start investigation of the intercalation, single-layer insertion, first. The intercalation into the graphite is unstable since the reconstruction energy of Na bulk and graphite are higher than the binding energy of Na–C[33]. Even so, Na may be intercalated into the graphitic domains of HC with less organized graphene sheets lowering the reconstruction energy. Thus, we estimate the formation energy of the Na-graphite intercalation compounds (Na-GICs) with different stacking of graphite (AB- and AA-stacking) as shown in Fig. 2. The stacking of graphite indicates the alignment of the carbon layers directly attached. For example, the sequence of stage II Na-GIC (AB) and Na-GIC (AA) are ANaABNaB and ANaAANaA, respectively, where A and B represent the graphene layers. The stacking order of the carbon layers around intercalated Na atom is fixed in the AA-sequence because Na prefers to intercalated between the AA-stacking graphite layers. The formation energy (E_{form}) is defined as

$$E_{\mathrm{form}} = E_{\mathrm{Na-C}} - n_{\mathrm{C}}\mu_{\mathrm{C}} - n_{\mathrm{Na}}\mu_{\mathrm{Na}}, \quad (1)$$

where $E_{\mathrm{Na\text{-}C}}$ is the total energy of the sodiated carbon (product), and n_i and μ_i are the number and chemical potential of the species i (i = C or Na). For the intercalation, the chemical potentials are set to the atomic energy of AB-stacking graphite and BCC Na metal, respectively. We use the identical Na chemical potential throughout the work to compare with the Na metal deposition/dissolution that should be avoided for battery safety. Here, we focus on NaC_8 series because NaC_6 series (0.147 eV per f.u. for stage I and 0.071 eV per f.u. for stage II) are less stable than NaC_8 series (0.129 eV per f.u. for stage I and 0.048 eV per f.u. for stage II), which is in agreement with the other theoretical studies[29,33].

Consistent with the previous studies summarized in Supplementary Table 1[29,30,33], the positive formation energies are observed, indicating that Na intercalation into graphite is not preferred. Nonetheless, it looks available that Na is stored in the graphitic domains of HC in two aspects, except for stage I. One is the stacking order of the graphitic domains would not be perfect like graphite because of disordered and partially curved graphene sheets in HC. In Fig. 2a, the formation energy of Na-GICs (AA) is lower than that of AA-stacking graphite, which shows that Na

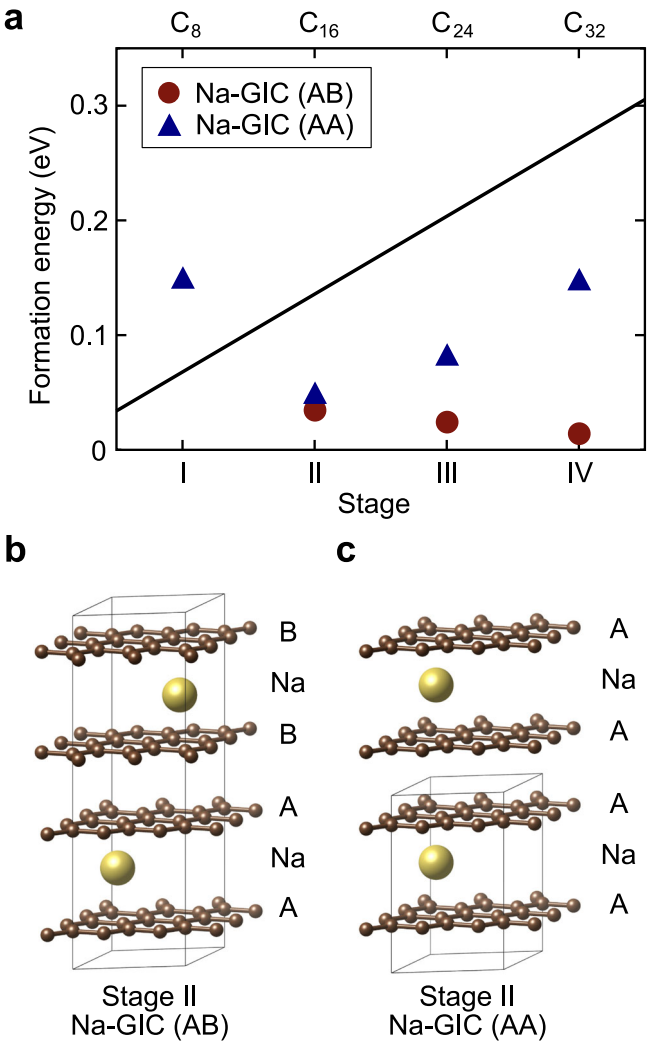

Fig. 2 Formation energy and structures of Na-GICs. a The formation energy of Na-GICs with respect to AB-stacking graphite and BCC Na metal. The dashed line indicates the formation energy of AA-stacking graphite. Schematic structures of stage II Na-GIC with **b** AB-stacking and **c** AA-stacking.

intercalation into the AA-stacking graphite is energetically favorable. Therefore, intercalation can occur in the graphitic domains which have less stable stacking. The other aspect is the wide interlayer distance (d_{int}) of graphitic domains, reported to be 3.6–4.0 Å[21,23,37] exceeding d_{int} of graphite (3.35 Å). The energy to widen the interlayer distance of AB-stacking graphite to 3.75 Å is 5.5 meV per atom as shown in Supplementary Fig. 2. Therefore, the reconstruction energy of intercalant layer (NaC_8 series) is reduced by 44 meV, which is enough to overcome the positive formation energy of Na-GICs (AB). Thus, Na can be intercalated even into the AB-stacking graphitic domains. It is in agreement with the previous study[38] using bilayer model that Na can be stored in the graphitic domain with wide interlayer space or AA-stacking. However, the highly unstable formation energy of stage I Na-GIC implies that the intercalation capacity is not enough to explain the capacity of typical HC. (The origin of instability of stage I Na-GIC can be seen in Supplementary Note 1.) As a result, in the HC, Na can be intercalated into the graphitic domains with less aligned carbon layers and wider interlayer spacing than pure graphite, up to the theoretical capacity of 140 $mAhg^{-1}$ corresponding to stage II (NaC_{16}).

Then, we estimate the cell potential vs. Na/Na^+ to identify the related region among the plateau and slope regions. In case the x Na^+ ions are stored in the host crystal with $Na_{n-x}C_m$ forming a new structure with Na_nC_m (x, n and m are the number of atoms), the average cell potential can be calculated using the following equation[39].

$$V(x) = -\frac{E(\mathrm{Na}_n\mathrm{C}_m) - E(\mathrm{Na}_{n-x}\mathrm{C}_m) - x\mu_{\mathrm{Na}}}{xe} = -\frac{E_{\mathrm{form}}(\mathrm{Na}_n\mathrm{C}_m) - E_{\mathrm{form}}(\mathrm{Na}_{n-x}\mathrm{C}_m)}{xe}, \quad (2)$$

where E and E_{form} indicate the total energy and the formation energy of each structure, respectively. In the intercalation of Na into the AA-stacking graphite, the average cell potential can be estimated from the formation energy of AA-stacking graphite (dashed line) and Na-GIC (AA) (blue triangle) in Fig. 2a. Here, the difference is about 0.1 eV corresponding to the voltage of plateau region (0–0.1 V). Also, the cell potential does not exceed 0.2 V regardless of stacking order even though we assume the wide interlayer distance of 4.0 Å. As a result, intercalation is one of the components of plateau capacity between 100 and 300 $mAhg^{-1}$ in Fig. 1c.

Na adsorption on the pore wall of pristine and defective graphene

The adsorption on the pore wall is regarded as another Na-storing mechanism. Since the micropores are surrounded by graphitic domains, graphene model is used as pore wall for the studies of Na adsorption as shown in Fig. 3a. Fortunately, the influence of the number of graphene layers is not significant as discussed in Supplementary Table 4 and Supplementary Fig. 3 so we can use graphene sheet instead of the (0001) surface of graphite. Although the adsorption is considered as possible sodiation mechanism, several studies have reported that Na is unstable to be adsorbed on the pristine (defect-free) graphene and can only be adsorbed on the defective graphene[29,34,38,40]. Therefore, for a high capacity of Na, at least one of the conditions must be satisfied: HC has a sufficiently high defect concentration or multiple atoms (e.g. Na clusters) are adsorbed on one defect. Here, we focus on the adsorption of Na cluster on defective graphene, such as Stone-Wales (SW), mono-vacancy (MV), and di-vacancy (DV). The influence of electrolyte is not taken into account, so this system is close to the pore wall of the micropores where electrolyte is barely penetrated. In order to evaluate that Na cluster can be adsorbed on the defective graphene, we estimate the formation energy (E_{form}) using Eq. (3),

$$E_{\mathrm{form}} = E_{\mathrm{Na-graphene}} - E_{\mathrm{graphene}} - n_{\mathrm{Na}}\mu_{\mathrm{Na}}, \quad (3)$$

where $E_{Na\text{-}graphene}$ and $E_{graphene}$ are the total energy of the Na adsorbed graphene and pristine or defective (SW, MV, DV) graphene, and the others are consistent with the Eq. (1). To simulate the adsorption of Na on the defective graphene, 6 × 6 supercell (72 atoms) is used because the defect formation energies in the cell are in good agreement with the experiment. (See Supplementary Table 2) The island-shape Na clusters in the previous study[34] are chosen as initial structures. The optimized structures of the Na cluster on the pristine graphene are presented in the inset of Fig. 3b. In addition, we display the geometries of the Na cluster on defective graphene in Supplementary Fig. 2, in which the structures of the cluster are almost preserved even on the defective graphene.

Figure 3b shows that single-atom adsorption on the defect sites is always stable. Even though the numerical values are slightly different, the sign and trend are consistent with the previous study[29] (see Supplementary Table 3). In addition, island-shape small-size cluster (Na_4) on the defective graphene is more energetically stable than single atom. This result shows that additional Na ions can be stored as a cluster. Whereas, the adsorption of island-shape Na_{10} cluster is always much less stable than Na_4 cluster. Furthermore, the formation of Na layers completely covering the pristine graphene (Na plating) is also always unstable regardless of the thickness of Na layers as shown in Supplementary Table 4. Therefore, large-size Na cluster cannot be adsorbed even on the defective graphene of pore wall. By the way, the formation energies in this work are less stable compared to the previous study[34] using DFT-D2 method for vdW-correction. This is because the Li adsorption energy on graphene with DFT-D2 is much more stable than the energy using other vdW schemes[29]. Therefore, the stability of island-shaped Na cluster on the graphene might be exaggerated in the previous study.

The adsorption energy of the first Na atom on the MV and DV graphene is quite low about −1 eV so it is one of the origins of slope capacity with 0.1–1.5 V vs Na/Na^+. Whereas, the change of formation energy is below 0.1 eV for additional Na of the cluster. Therefore, clustering on the defective surface contributes to the plateau capacity along with intercalation. SW defect is also related to the plateau capacity. As a result, Na adsorption on defective graphene can contribute to both the slope capacity and the plateau capacity.

Na storage in micropore via pore-filling

Next, we evaluate whether pore-filling that Na ions fully occupy the micropore beyond adsorption on the pore wall can occur. In this study, we use the slit-shaped pore based on the experimental observation of the presence of flat carbon fragments[41,42]. Consistent with the adsorption calculation, it is possible to use the slit-shaped pore with two layers of graphene in Fig. 3a which can minimize the computation cost. In the slit-shaped pore, slab-like Na cluster (Na slab) would be formed completely to fill the pore. Therefore, we use graphene-Na slab-graphene sandwich model as displayed in the inset of Fig. 3c where the structure of each Na layer is consistent with Li in LiC_6. The optimized Na–Na bond length is about 3.7 Å that is similar to the experimental bond length of BCC metal. We also consider the slab structure based on the Na layer in NaC_8 but it is less stable. The formation energy is calculated by using Eq. (1) where μ_C is corresponded to the energy of graphene since we assume that Na ions are stored in the separated graphene sheets where the interaction energy between graphene sheets is almost negligible.

As shown in Fig. 3c, Na slab in the pore with pristine graphene is stable if the slab thickness is lower than 6 layers (1.87 nm), in contrast to the unstable Na plating. Especially, 3–4 layers of Na slab would be more favorable due to its completely stable formation energy. However, the Na slab in the pore becomes less

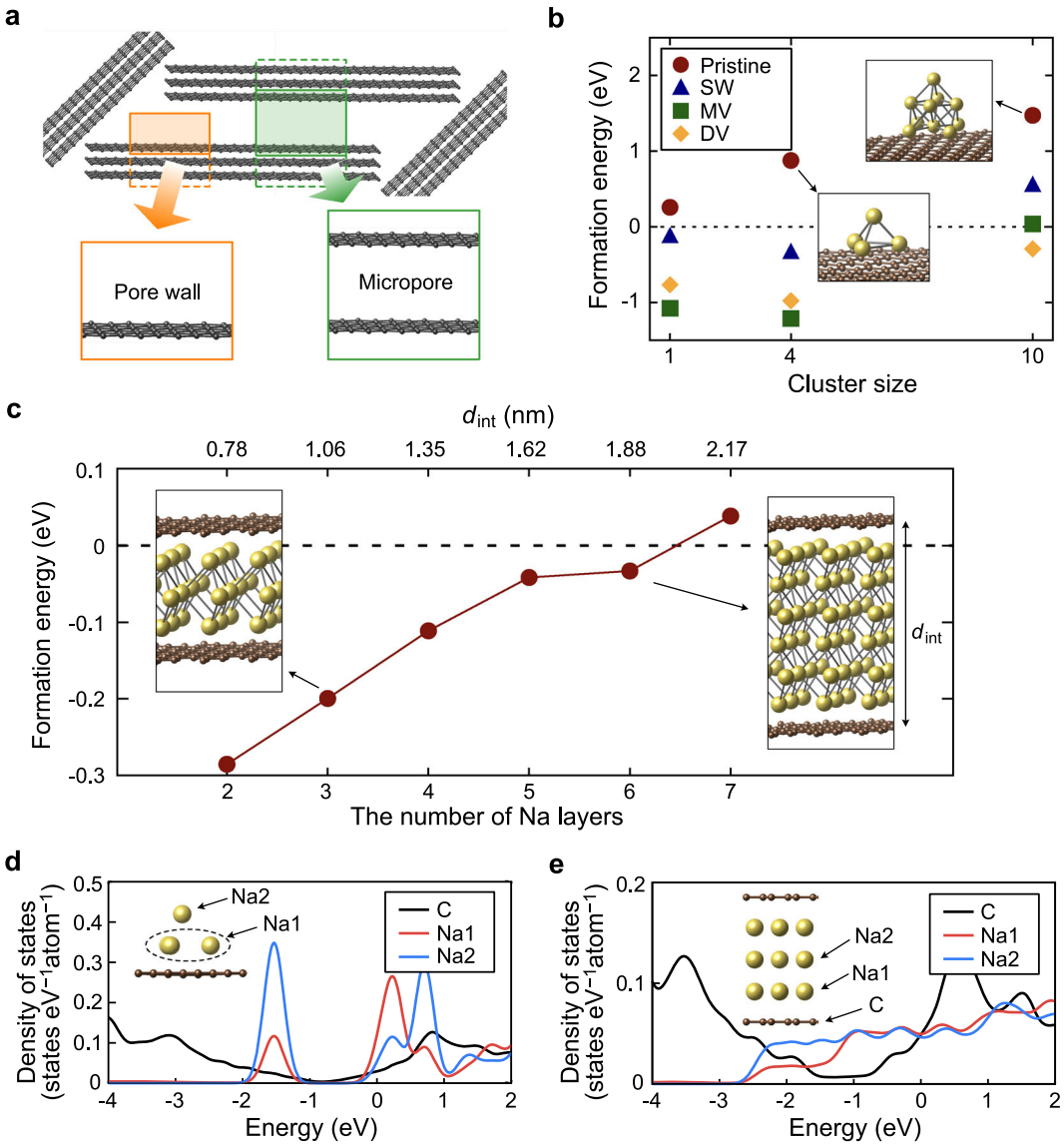

Fig. 3 Formation energy and density of states of Na cluster in micropore. a Schematic figure of micropore surrounded by graphitic domains. Simplifying the geometry, single-layer graphene is used instead of graphite. The formation energy of **b** the adsorption of Na cluster on the various defective graphene and **c** Na slab inside slit-shaped graphene pore. Projected density of states of **d** Na cluster on graphene and **e** Na slab inside slit-shaped pore (Fermi level is set to 0). Insets show the Na–C structures.

stable by increasing the slab thickness and eventually becomes unstable when the thickness exceeds 7 layers (2.17 nm) since the Na slab, hexagonal crystal, is a metastable configuration. The result shows that Na ions can be stored in pores, especially micropores, as nanometer-size clusters. In the 3-–6 layers of Na slab, the averaged formation energy per Na atom is lower than 0.1 eV, indicating that nanometer-size Na clusters in micropores can increase the plateau capacity ($0 < V < 0.1$ V).

By the way, this result does not indicate that the Na slab can be formed in the graphitic domains. Although the sandwich structure is more stable than Na metal and the separated carbon layers, it is less stable than Na metal and bilayer graphite (or graphite) due to the energy cost to expand the interlayer distance. Nonetheless, it is interesting that the Na-rich stage II Na-GIC where two layers Na slab is filled in the intercalant layer is more stable than stage I Na-GIC, in agreement with the experiment under high-pressure condition with molten Na[43].

Electronic structure of Na–C system

The charge states of stored Na cluster are also interesting. Figure 3d, e shows the projected density of states (PDOS) of Na atoms stored in carbon materials. For detailed analysis, we provide separated PDOS of Na according to the distance from graphene sheets. In the metal intercalated graphite[33], the conduction bands of carbon are partially occupied due to the electrons transferred from metal. As shown in Fig. 3d, the graphene where island-shape Na cluster is adsorbed also has partially occupied conduction bands similar to the metal intercalated graphite. Also, we can observe a small number of states of the Na atoms directly adsorbed on the graphene (Na1) below the fermi level like the positively charged metals intercalated into the graphite. However, the Na atom far from graphene (Na2) is different from the directly adsorbed one. It rarely loses its electron and exists in a quasi-neutral charge state.

Similar to the Na cluster adsorbed on the graphene, directly adsorbed Na (Na1) in the slit-shaped pore donates electrons to

carbon layers as shown in Fig. 3e. Whereas, Na at the middle of the slab (Na2) still has occupied states even below the energy level corresponding to the Fermi level in pure graphene. It shows that the charge state of Na is almost neutral, except for the Na atoms directly contacted to graphene. The partial atomic charges in Supplementary Table 5 also demonstrate the results consistent with PDOS analysis that Na2 is less positive than Na1. Therefore, the size-limited Na clusters in micropores can be the origin of quasi-metallic peak (6/7Li NMR 760 ppm chemical shift) in the experiment[44]. In addition, the quasi-metallic peak observed in plateau region is consistent with our result that cluster adsorption and pore-filling are related to the plateau capacity. By contrast, it is already known that the high reactivity of Na metal plate with liquid electrolytes hinders the practical applications of Na metal anode. However, in our case, quasi-metallic Na atoms are placed in the micropore where the liquid electrolytes cannot penetrate. Therefore, it is free from the issue.

Sodiation mechanism of hard carbon

Figure 4 shows the charge–discharge curve with corresponding mechanism to the plateau and slope capacity. The slope region is related to the defect or edge. With the adsorption on the defect in the pore wall, the adsorption on the edge sites and the intercalation into the graphitic domains with defect also contribute to the slope capacity (see Supplementary Note 2). Therefore, it is expected that the slope capacity has a positive correlation with the defect concentration, which is in good agreement with the experiment[21,37].

On the other hand, Na ions intercalated into the graphitic domains and Na cluster from the adsorbed Na on the defect result in the plateau capacity. As we discussed, intercalation into the HC with typically reported interlayer distance over 3.75 Å[21,23,37] is always energetically stable. Therefore, interlayer distance could not be an indicator for intercalation capacity unless the graphitic domain has both a much narrower distance than typical HC and a highly aligned AB-staking order. Instead, narrow interlayer distance reduces the formation energy difference (close to zero), resulting in the low plateau potential[37]. Therefore, in the typical HC with the turbostratic structure and sufficient interlayer distance, the large size of graphitic domains and low defect concentration seem more important to increase the intercalation capacity.

Na clusters in the close micropore for electrolyte also contribute to the plateau capacity. Therefore, large close pore volume is necessary for high capacity. In experiment, pore volume measured by N_2 gas is reduced with the increase in temperature for heat-treated HC. However, the decrease of skeletal density implies the increase of the close pore volume in contrast to the measured pore volume[37,45,46]. Therefore, it is expected that Na cluster in the pore is still one of the component of plateau capacity despite its small pore volume measured by N_2 gas. Instead, the HC at low temperature has much poorer plateau capacity, which can be figured out through the highly defective small-size graphitic domains reducing intercalation capacity and larger open pore volume related to the irreversible capacity.

We showed that not only island-shape Na cluster adsorption on the pore wall but pore-filling is energetically stable via the sandwich model. In addition, it was demonstrated that Na ions will easily diffuse on the graphene[40] and in the Na-GIC[47] according to the migration activation energy. However, the capacity in the typical studies is much lower than expected one assuming from close pore volume, suggesting that pore-filling, excluding the adsorption at the pore wall, poorly contributes to the capacity in the typical HC. As a result, during charge process, Na ions are first stored at the defect-related sites as shown in Fig. 4 (red line). Then, Na ions are intercalated into the graphitic domains or make island-shape clusters adsorbed on the pore wall until the capacity becomes about 300 mAhg^{-1} (blue line).

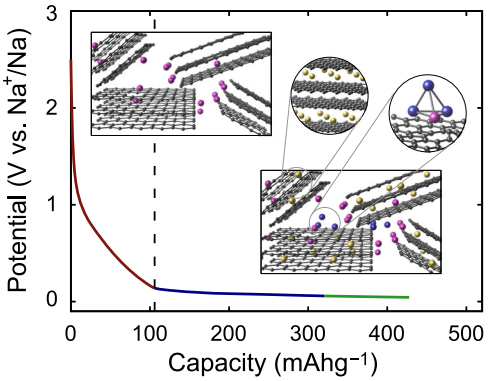

Fig. 4 Identified sodiation mechanism of HC. Schematic diagram of charge–discharge curve with the related mechanism.

Mechanism of micropore filling

We mentioned that the contribution of pore-filling in the typical HC is poor in spite of the negative formation energy of the sandwich model. However, it is difficult to explain the extended capacity of over 400 mAhg^{-1} in the recent work[36] (green line in Fig. 4) from the above mechanism excluding pore-filling due to the impossible stage I Na-GIC and the limited cluster size. Whereas, pore-filling could be a key factor to increase the capacity because one Na is stored for every two carbons in the case of the thickest Na slab (6 layers) among the stable. Thus, we perform deep analysis to understand pore-filling mechanism how to grow from island-shape small-size cluster in Fig. 3b to nanometer-size cluster (or Na slab) in Fig. 3c.

Assuming the procedure to fill the pore with Na ions, initially, the ions should be adsorbed on the pore wall. In addition, Na ions have to be collected and build Na cluster to fill the pore. However, Na ions cannot be adsorbed on the pore wall without defects due to the positive adsorption energy on the pristine graphene. Even on defective graphene, only two layers of Na clusters (Na_4) can be formed. Therefore, it is difficult to fill the pore with 4 or more layers of Na slab in the slit-shaped pore with one defect since there is no cluster on the defect-free side of the wide slit. Whereas, Na slab with three layers may be formed in the narrow slit-shaped pore with one defect because the additional ions beyond two layers of Na cluster on the defective site reach directly to the pristine graphene on the other side, which can stabilize the system.

Figure 5a shows the formation energy of island-shape Na clusters between the defective graphene layer and pristine graphene layer. The initial structure of Na_{14} cluster is built by imposing z-symmetry to Na_{10} cluster, and the geometry of a three-layer Na slab is used for Na_{24} cluster as shown in Fig. 5a (3-dimensional view) and Supplementary Fig. 4 (top view). The Na_{14} cluster looks like the conventional unit cell of FCC. The size of graphene for Na_{14} is the same as that used for the adsorption (72 carbons for each graphene). Whereas, we use larger size of graphene with 128 atoms for Na_{24}. The width of pore is fixed as 1.08 nm considering the three-layer Na slab model. Na_{14} cluster intercalated into the slit-shaped pore has compatible formation energy with Na_4 cluster on the defective graphene surface. Therefore, pore filling with the three-layer cluster (or slab) seems to be possible unlike the Na_{10} adsorption on the graphene surface. In addition, if we consider the effect of the thickness of the graphitic domains surrounding pore in the previous chapter, Na_{14} on the multi-layered pore wall, close to the real situation, would be more stable.

For detailed analysis, we calculate the energy by changing the pore width in Fig. 5b. The formation energy of Na_4 cluster on graphene is

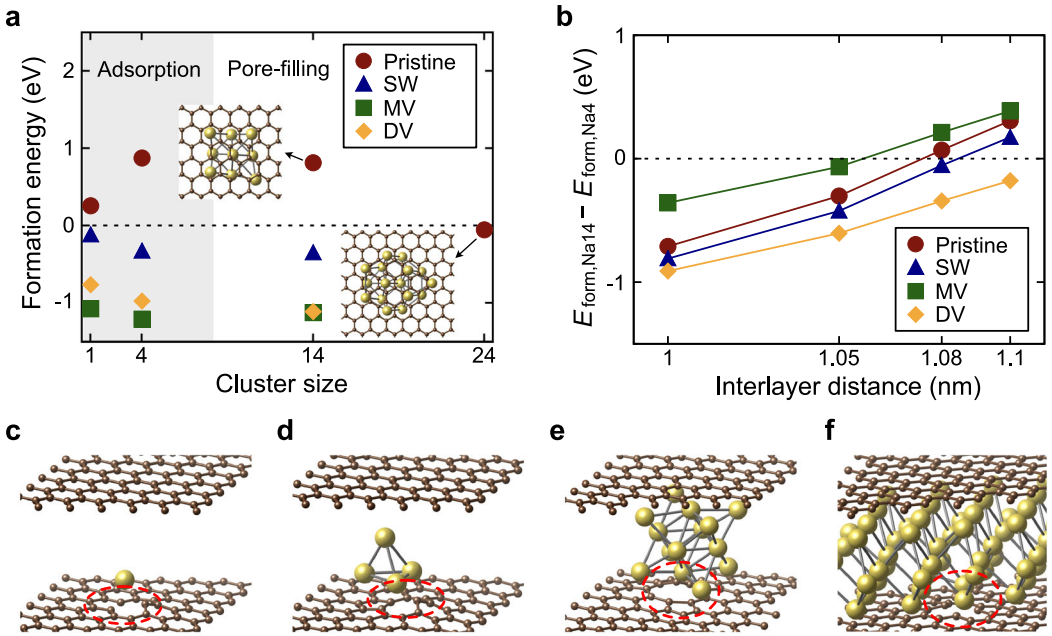

Fig. 5 Pore-filling mechanism in micropore and correlated formation energy. a The formation energy of Na cluster inside slit-shaped graphene pore according to the cluster size. For the small cluster in shade region, adsorption energy is displayed. **b** The difference of formation energy between Na_{14} cluster inside the pore and Na_4 on the graphene as a function of interlayer distance. **c**–**f** Structures of Na-storing slit-shaped graphene pore with mono-vacancy.

used as reference energy. In the pristine graphene, the optimized distance is 0.91 nm that is shorter than 3 layers slab model. Therefore, the structures become more stable by reducing the interlayer distance. Especially, below 1.05 nm, Na_4 cluster on the graphene can always grow to Na_{14} cluster inside pore. In addition, negative formation energy of Na_{24} was observed in Fig. 5a, which implies that adsorbed cluster on the defect site can grow in the lateral direction like 3 layers slab model. The formation energy difference between Na_4 on graphene and Na_{14} in pore is below 0.1 eV per atom. Thus, it can be a reasonable source of the plateau capacity. As a result, during the charge process, Na ions can fill the pore in the form of Na three-layer slab using the following mechanism:

(1) Adsorption of Na atom on the pore wall of defective graphene surface (Fig. 5c).
(2) Growth of island-shape Na cluster from adsorbed atom (Fig. 5d, e).
(3) Lateral growth of Na cluster to fill the slit-shaped pore with nanometer-size Na slab (Fig. 5f).

DISCUSSION

Our study has led to a design principle for high capacity in which HC structure should have slightly defective large graphitic domains and a plenty of small-size pores. In the most of the previous studies, annealing temperature is used to control the geometry of HC. However, it is difficult to get the optimized HC adjusting the annealing temperature since the high temperature enlarges and thickens graphitic domains, leading to small total pore volume and large-size pore[37]. One approach to overcome the problem is making pore after constructing carbon frameworks. MgO-templated HC looks like that material following this approach and it achieved outstanding capacity with over 400 $mAhg^{-1}$ [36].

In the experiment, HCs were synthesized using the mixture of Mg gluconate and glucose. After mixing, pre-annealing was performed to make the carbon structure embedded MgO nanoparticle. The presence of MgO nanoparticle was confirmed from the experimental observation. Then, MgO nanoparticles were removed out during post heat treatment at 1500 °C which seems sufficient temperature to build large and less defective turbostratic carbon frameworks but not to fill the embedded pores. Figure 6 shows the MgO-templated HC structures using DFT-based Car-Parrinello Molecular Dynamics[48] simulations. In spite of the limited system size, we can observe the graphite-like regions consisting of over two layers of graphene and micropore. In addition, most of the carbon atoms (~95%) are threefold coordinated sp^2 configuration, which is in good agreement of the experiment. The size of pore is about 1 nm corresponding to the distance between graphene layers with three layers of MgO particle, which is also consistent to the interlayer spacing of the sandwich model with three layers Na slab that is the optimal size in our mechanism.

Interestingly, the optimal size is the internal pore size (~1.1 nm) of the hand-ground 50:50 mol/mol mixture of Mg gluconate and glucose which provides the highest capacity. In addition, even though the exact close pore volume is unknown, the 50:50 mol/mol mixture can be expected to have a larger close pore volume than HC from pure glucose because the measured volume of open pores, which are probably generated by crushing particles, increases from almost zero to about 0.5 $cm^3\ g^{-1}$. Therefore, we can suppose that the Na clusters filling the pores can lead to the excess plateau capacity. This result is in good agreement with our expectation and it shows that the internal pore could be a key for high-capacity HC. On the other hand, there is no increasement of the capacity in the HC using pure Mg glucose though its pore volume (over 0.2 $cm^3\ g^{-1}$) is larger than the 50:50 HC. According to our pore-filling mechanism, pore-filling is almost impossible when the pore size is larger than 1.1 nm. Thus, pore-filling cannot contribute to the capacity of the HC from pure Mg glucose with the pore size of 1.5 nm in spite of the large pore volume, which shows the validity of our mechanism. By the way, the freeze-drying HC from pure Mg gluconate has much poorer plateau capacity and higher irreversible capacity than any other HC. We mentioned that less defective large graphitic domains are one of the components for high capacity. Therefore, the barely constructed graphitic domains of the pure Mg gluconate freeze-drying HC can result in quite low plateau capacity. Also, the lack of the graphitic

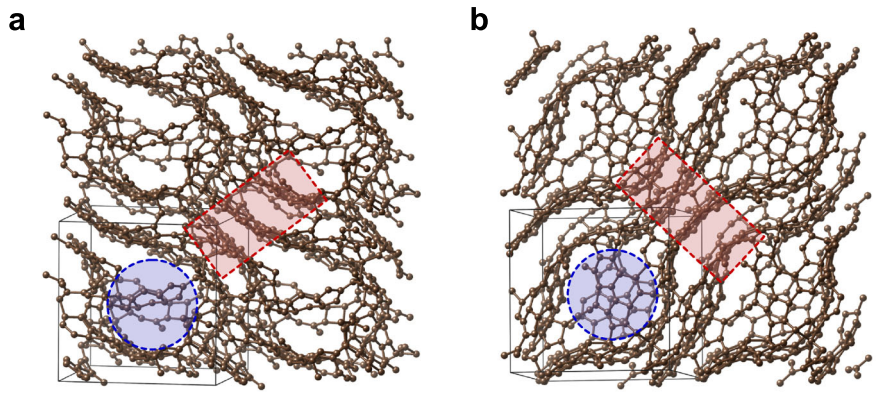

Fig. 6 The structure of MgO-templated HC. The structures of MgO-templated HC from the different initial structures. To show the graphite region, we present $2 \times 2 \times 1$ supercell. The solid black line indicates the unit cell. Red box and blue circle show the graphite-like region and pore region, respectively.

domains can make the pores be easily exposed to the electrolytes and increase irreversible capacity.

In summary, we revealed the sodiation mechanism of HC via DFT calculations. We clarified that intercalation into the graphitic domains and cluster formation in the micropores are the origin of the plateau capacity. In particular, we demonstrated that not only island-shape small-size clusters on the pore wall also nanometer-size Na clusters with 3–6 layers in the micropore are energetically favorable. Especially, 3–4 layers of Na slab could be a dominant size in terms of the energetics. The finding well explains the extended plateau capacity beyond typical 300 $mAhg^{-1}$, up to 478 $mAhg^{-1}$ recently achieved in MgO-templated HC. Furthermore, we clarified that MgO-templated HC can give many micropores suitable for nanometer-size Na cluster with slightly defective graphitic domains. Last, we believe that the present work can help theoretically to design high-capacity HC and improve the atomistic theory of complicated HC science.

METHODS

DFT calculations

All calculations are performed using density functional theory implemented in Vienna Ab-initio Simulation Package[49]. We use the generalized gradient approximation with Perdew, Burke, and Ernzerhof (PBE) functional[50] and with the vdW-optPBE functional[51]. The vdW-optPBE is chosen for the van der Waals correction because it produced reasonable results in the previous studies for the Li-graphite system[29,30,33]. The cutoff energy for plane-wave basis set is set to be 450 eV and the k-points are sampled as Γ-centered grid with a k-point spacing smaller than 0.042 $Å^{-1}$. The spin-polarization is considered. Also, the dipole correction is applied for the adsorption of Na cluster or Na atom on the graphene. Atomic positions are optimized until the forces at each atom are converged to within 1 meV·$Å^{-1}$. Also, we perform the cell optimization to estimate the Na intercalation energy into graphite. Whereas, we use fixed cell for the graphene as the optimized geometry in the graphite.

Structure modeling for MgO-templated hard carbon

We carry out molecular dynamic simulation using Car-Parrinello molecular dynamics (CPMD) code[48]. PBE functional is used for exchange-correlation and the semi-empirical Grimme D2 correction[52] is applied for the van der Waals correction. Cutoff energy is set to be 90 Ry. For initializing the MgO-templated HC structure, we first generate carbon supercell where 310 carbon atoms are randomly distributed in the cubic cell of 1.4 nm at the density of graphite (2.25 g·cm^{-3}). Then, MgO nanoparticle (18 formula units) is inserted removing the carbon atoms in the selected region. The structure is annealed for about 40 ps at 2500 K using Nose thermostat with the frequency of 1500 cm^{-1}. The atomic positions of MgO nanoparticle are fixed during annealing. Afterward, we remove the MgO nanoparticle and then perform annealing for about 20 ps at 2000 K.

In the experiment, pre-annealing was performed at low temperature and the high-temperature annealing was carried out after removing the MgO particle. However, it is difficult to perform the simulation for a long time to generate the well-organized graphene sheets below the temperature to fill the pore. Therefore, we perform the high-temperature annealing with fixed MgO nanoparticle to keep the pore and make well-aligned graphene sheets. In addition, final structures after post-annealing show that the micropore will not disappear after post-annealing in the experiment.

DATA AVAILABILITY

All data sets used in this work are available from the corresponding author on reasonable request.

Received: 26 August 2020; Accepted: 8 March 2021;
Published online: 09 April 2021

REFERENCES

1. Nishi, Y. The development of lithium ion secondary batteries. *Chem. Rec.* **1**, 406–413 (2001).
2. Yoshino, A. The birth of the lithium-ion battery. *Angew. Chem. Int. Ed.* **51**, 5798–5800 (2012).
3. Nitta, N., Wu, F., Lee, J. T. & Yushin, G. Li-ion battery materials: present and future. *Mater. Today* **18**, 252–264 (2015).
4. Roberts, S. & Kendrick, E. The re-emergence of sodium ion batteries: testing, processing, and manufacturability. *Nanotechnol. Sci. Appl.* **11**, 23–33 (2018).
5. Palomares, V. et al. Na-ion batteries, recent advances and present challenges to become low cost energy storage systems. *Energy Environ. Sci.* **5**, 5884 (2012).
6. Yabuuchi, N., Kubota, K., Dahbi, M. & Komaba, S. Research development on sodium-ion batteries. *Chem. Rev.* **114**, 11636–11682 (2014).
7. Yoshida, H. et al. P2-type $Na_{2/3}Ni_{1/3}Mn_{2/3-x}Ti_xO_2$ as a new positive electrode for higher energy Na-ion batteries. *Chem. Commun.* **50**, 3677–3680 (2014).
8. Wang, T. et al. Electrode materials for sodium-ion batteries: considerations on crystal structures and sodium storage mechanisms. *Electrochem. Energy Rev.* **1**, 200–237 (2018).
9. Yazami, R. & Touzain, P. A reversible graphite-lithium negative electrode for electrochemical generators. *J. Power Sources* **9**, 365–371 (1983).
10. Wen, Y. et al. Expanded graphite as superior anode for sodium-ion batteries. *Nat. Commun.* **5**, 1–10 (2014).
11. Irisarri, E., Ponrouch, A. & Palacin, M. R. Review-hard carbon negative electrode materials for sodium-ion batteries. *J. Electrochem. Soc.* **162**, A2476–A2482 (2015).
12. Dahbi, M., Yabuuchi, N., Kubota, K., Tokiwa, K. & Komaba, S. Negative electrodes for Na-ion batteries. *Phys. Chem. Chem. Phys.* **16**, 15007 (2014).
13. Dou, X. et al. Hard carbons for sodium-ion batteries: structure, analysis, sustainability, and electrochemistry. *Mater. Today* **23**, 87–104 (2019).
14. Chen, X. et al. High-performance sodium-ion batteries with a hard carbon anode: transition from the half-cell to full-cell perspective. *Nanoscale* **11**, 22196–22205 (2019).
15. Wahid, M., Puthusseri, D., Gawli, Y., Sharma, N. & Ogale, S. Hard carbons for sodium-ion battery anodes: synthetic strategies, material properties, and storage mechanisms. *ChemSusChem* **11**, 506–526 (2018).

16. Stevens, D. A. & Dahn, J. R. High capacity anode materials for rechargeable sodium-ion batteries. *J. Electrochem. Soc.* **147**, 1271 (2000).
17. Komaba, S. et al. Electrochemical Na insertion and solid electrolyte interphase for hard-carbon electrodes and application to Na-Ion batteries. *Adv. Funct. Mater.* **21**, 3859–3867 (2011).
18. Bommier, C., Surta, T. W., Dolgos, M. & Ji, X. New mechanistic insights on Na-ion storage in nongraphitizable carbon. *Nano Lett.* **15**, 5888–5892 (2015).
19. Morita, R. et al. Combination of solid state NMR and DFT calculation to elucidate the state of sodium in hard carbon electrodes. *J. Mater. Chem. A* **4**, 13183–13193 (2016).
20. Li, Z. et al. Mechanism of Na-ion storage in hard carbon anodes revealed by heteroatom doping. *Adv. Energy Mater.* **7**, 1602894 (2017).
21. Qiu, S. et al. Manipulating adsorption–insertion mechanisms in nanostructured carbon materials for high-efficiency sodium ion storage. *Adv. Energy Mater.* **7**, 1–11 (2017).
22. Anji Reddy, M., Helen, M., Groß, A., Fichtner, M. & Euchner, H. Insight into sodium insertion and the storage mechanism in hard carbon. *ACS Energy Lett.* **3**, 2851–2857 (2018).
23. Alvin, S. et al. Revealing sodium ion storage mechanism in hard carbon. *Carbon N. Y.* **145**, 67–81 (2019).
24. Wang, K. et al. Sodium storage in hard carbon with curved graphene platelets as the basic structural units. *J. Mater. Chem. A* **7**, 3327–3335 (2019).
25. Xiao, B., Rojo, T. & Li, X. Hard carbon as sodium-ion battery anodes: progress and challenges. *ChemSusChem* **12**, 133–144 (2019).
26. Zhang, B., Ghimbeu, C. M., Laberty, C., Vix-Guterl, C. & Tarascon, J.-M. Correlation between microstructure and Na storage behavior in hard carbon. *Adv. Energy Mater.* **6**, 1501588 (2016).
27. Morita, R. et al. Correlation of carbonization condition with metallic property of sodium clusters formed in hard carbon studied using ^{23}Na nuclear magnetic resonance. *Carbon* **145**, 712–715 (2019).
28. Gotoh, K. et al. Mechanisms for overcharging of carbon electrodes in lithium-ion/sodium-ion batteries analysed by operando solid-state NMR. *J. Mater. Chem. A* **8**, 14472–14481 (2020).
29. Tsai, P., Chung, S., Lin, S. & Yamada, A. Ab initio study of sodium intercalation into disordered carbon. *J. Mater. Chem. A* **3**, 9763–9768 (2015).
30. Moriwake, H., Kuwabara, A., Fisher, C. A. J. & Ikuhara, Y. Why is sodium-intercalated graphite unstable? *RSC Adv.* **7**, 36550–36554 (2017).
31. Lenchuk, O., Adelhelm, P. & Mollenhauer, D. New insights into the origin of unstable sodium graphite intercalation compounds. *Phys. Chem. Chem. Phys.* **21**, 19378–19390 (2019).
32. Liu, Y., Merinov, B. V. & Goddard, W. A. Origin of low sodium capacity in graphite and generally weak substrate binding of Na and Mg among alkali and alkaline earth metals. *Proc. Natl Acad. Sci. USA* **113**, 3735–3739 (2016).
33. Wang, Z., Selbach, S. M. & Grande, T. Van der Waals density functional study of the energetics of alkali metal intercalation in graphite. *RSC Adv.* **4**, 4069–4079 (2014).
34. Liang, Z., Fan, X., Zheng, W. & Singh, D. J. Adsorption and formation of small Na clusters on pristine and double-vacancy graphene for anodes of Na-ion batteries. *ACS Appl. Mater. Interfaces* **9**, 17076–17084 (2017).
35. Dimakis, N. et al. Li and Na adsorption on graphene and graphene oxide examined by density functional theory, quantum theory of atoms in molecules, and electron localization function. *Molecules* **24**, 754 (2019).
36. Kamiyama, A. et al. MgO-template synthesis of extremely high capacity hard carbon for Na-ion battery. *Angew. Chem. Int. Ed.* **60**, 5114–5120 (2021).
37. Kubota, K. et al. Structural analysis of sucrose-derived hard carbon and correlation with the electrochemical properties for lithium, sodium, and potassium insertion. *Chem. Mater.* **32**, 2961–2977 (2020).
38. Bommier, C., Ji, X. & Greaney, P. A. Electrochemical properties and theoretical capacity for sodium storage in hard carbon: insights from first principles calculations. *Chem. Mater.* **31**, 658–677 (2019).
39. Aydinol, M. K., Kohan, A. F., Ceder, G., Cho, K. & Joannopoulos, J. Ab initio study of lithium intercalation in metal oxides and metal dichalcogenides. *Phys. Rev. B* **56**, 1354–1365 (1997).
40. Olsson, E., Chai, G., Dove, M. & Cai, Q. Adsorption and migration of alkali metals (Li, Na, and K) on pristine and defective graphene surfaces. *Nanoscale* **11**, 5274–5284 (2019).
41. Petnikota, S., Rotte, N. K., Reddy, M. V., Srikanth, V. V. S. S. & Chowdari, B. V. R. MgO-decorated few-layered graphene as an anode for Li-ion batteries. *ACS Appl. Mater. Interfaces* **7**, 2301–2309 (2015).
42. White, R. J., Brun, N., Budarin, V. L., Clark, J. H. & Titirici, M.-M. Always look on the "light" side of life: sustainable carbon aerogels. *ChemSusChem* **7**, 670–689 (2014).
43. Udod, I. A. Sodium-graphite intercalation compound of the first stage: two-dimensional structure and stability. *Synth. Met.* **88**, 127–131 (1997).
44. Stratford, J. M., Allan, P. K., Pecher, O., Chater, P. A. & Grey, C. P. Mechanistic insights into sodium storage in hard carbon anodes using local structure probes. *Chem. Commun.* **52**, 12430–12433 (2016).
45. Li, Y. et al. Regulating pore structure of hierarchical porous waste cork-derived hard carbon anode for enhanced Na storage performance. *Adv. Energy Mater.* **9**, 1902852 (2019).
46. Hasegawa, G. et al. Studies on electrochemical sodium storage into hard carbons with binder-free monolithic electrodes. *J. Power Sources* **318**, 41–48 (2016).
47. Wang, Z., Ratvik, A. P., Grande, T. & Selbach, S. M. Diffusion of alkali metals in the first stage graphite intercalation compounds by vdW-DFT calculations. *RSC Adv.* **5**, 15985–15992 (2015).
48. Car, R. & Parrinello, M. Unified approach for molecular dynamics and density-functional theory. *Phys. Rev. Lett.* **55**, 2471–2474 (1985).
49. Kresse, G. & Furthmüller, J. Efficient iterative schemes for ab initio total-energy calculations using a plane-wave basis set. *Phys. Rev. B* **54**, 11169–11186 (1996).
50. Perdew, J. P., Burke, K. & Ernzerhof, M. Generalized gradient approximation made simple. *Phys. Rev. Lett.* **77**, 3865–3868 (1996).
51. Thonhauser, T. et al. Van der Waals density functional: self-consistent potential and the nature of the van der Waals bond. *Phys. Rev. B* **76**, 125112 (2007).
52. Grimme, S. Semiempirical GGA-type density functional constructed with a long-range dispersion correction. *J. Comput. Chem.* **27**, 1787–1799 (2006).

ACKNOWLEDGEMENTS

This work was supported in part by MEXT as Elements Strategy Initiative, Grant Number JPMXP0112101003, Program for Promoting Researches on the Supercomputer Fugaku (Fugaku Battery & Fuel Cell Project), Grant Number JPMXP1020200301, and by JSPS KAKENHI, Grant Number JP19H05815. The calculations were carried out on the supercomputers in NIMS and The University of Tokyo as well as Kyushu University. This research also used computational resources of the HPCI system through the HPCI System Research Project (Project IDs: hp190126, hp200131).

AUTHOR CONTRIBUTIONS

Y.Y. contributed to performing DFT calculation and wrote manuscript. B.G., A.K., K.K., and S.K. reviewed and discussed the results. Y.T. coordinated the whole work and wrote manuscript. All authors reviewed and commented on the manuscript.

COMPETING INTERESTS

The authors declare no competing interests.

ADDITIONAL INFORMATION

Supplementary information The online version contains supplementary material available at https://doi.org/10.1038/s41524-021-00515-7.

Correspondence and requests for materials should be addressed to Y.T.

Reprints and permission information is available at http://www.nature.com/reprints

Publisher's note Springer Nature remains neutral with regard to jurisdictional claims in published maps and institutional affiliations.